

Transiently Responsive Block Copolymer Micelles Based on *N*-(2-Hydroxypropyl)methacrylamide Engineered with Hydrolyzable Ethylcarbonate Side Chains

Sabah Kasmi,[†] Benoit Louage,[†] Lutz Nuhn,[†] Alexandra Van Driessche,[†] Jan Van Deun,[‡] Izet Karalic,[†] Martijn Risseuw,[†] Serge Van Calenbergh,[†] Richard Hoogenboom,[§] Riet De Rycke,^{||} Olivier De Wever,[‡] Wim E. Hennink,[⊥] and Bruno G. De Geest^{*,†}

[†]Department of Pharmaceutics, Ghent University, 9000 Ghent, Belgium

[‡]Laboratory of Experimental Cancer Research, Department of Radiation Oncology and Experimental Cancer Research, Ghent University Hospital, 9000 Ghent, Belgium

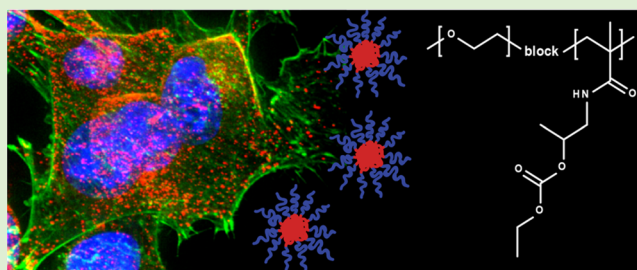
[§]Supramolecular Chemistry Group, Department of Organic and Macromolecular Chemistry, Ghent University, 9000 Ghent, Belgium

^{||}VIB inflammation Research Center, Zwijnaarde, 9052 Ghent, Belgium

[⊥]Department of Pharmaceutics, Utrecht Institute for Pharmaceutical Sciences, Utrecht University, 3512 JE Utrecht, The Netherlands

Supporting Information

ABSTRACT: The lack of selectivity and low solubility of many chemotherapeutics impels the development of different biocompatible nanosized drug carriers. Amphiphilic block copolymers, composed of a hydrophilic and hydrophobic domain, show great potential because of their small size, large solubilizing power and loading capacity. In this paper, we introduce a new class of degradable temperature-responsive block copolymers based on the modification of *N*-(2-hydroxypropyl)methacrylamide (HPMA) with an ethyl group via a hydrolytically sensitive carbonate ester, polymerized by radical polymerization using a PEG-based macroinitiation. The micellization and temperature-responsive behavior of the PEG–poly(HPMA-EC) block copolymer were investigated by dynamic light scattering (DLS). We observed that the polymer exhibits lower critical solution temperature (LCST) behavior and that above the cloud point (cp) of 17 °C the block copolymer self-assembles in micelles with a diameter of 40 nm. Flow cytometry analysis and confocal microscopy show a dose-dependent cellular uptake of the micelles loaded with a hydrophobic dye. The block copolymer nanoparticles were capable of delivering the hydrophobic payload into cancer cells in both 2D and 3D *in vitro* cultures. The block copolymer has excellent cytocompatibility, whereas loading the particles with the hydrophobic anticancer drug paclitaxel results in a dose-dependent decrease in cell viability.



INTRODUCTION

Chemotherapeutics, cytotoxic agents that act by killing rapidly proliferating cancer cells, suffer some major limitations.^{1,2} A primary limitation is the lack of selectivity toward cancer cells, being particularly harmful to rapidly proliferating healthy cells, such as blood cells, intestinal epithelial cells, and hair follicles. Consequently, side effects including anemia, nausea, and hair loss occur. Furthermore, many anticancer drugs have low solubility, which requires the use of organic solvents or surfactants (e.g., Cremophor EL (CrEL))³ to obtain a formulation that can safely be administered to patients.⁴ Paclitaxel (PTX), a clinically used neoplastic drug, was first isolated from the bark of the pacific yew, *Taxus brevifolia*, in 1962 by members of the National Cancer Institute.^{5,6} It is used to treat various cancers including ovarian, breast, and lung cancers, as well as Kaposi sarcoma. A major drawback is its low aqueous solubility of about 0.3 µg/mL. Consequently,

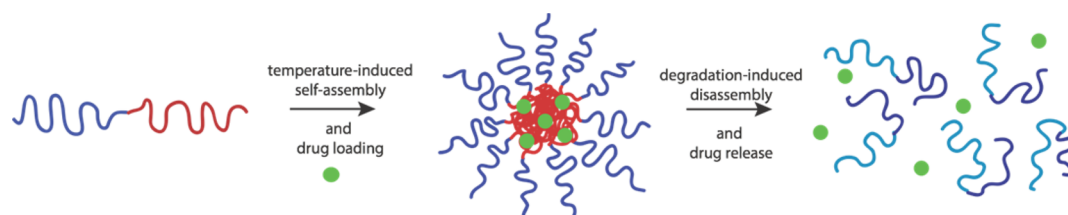
intravenous administration requires a mixture of 50% dehydrated ethanol and 50% CrEL as formulation vehicle.⁷ CrEL is a nonionic surfactant derived from castor oil and causes some serious side effects. The most well-known side effects of paclitaxel formulated with CrEL are anaphylactic hypersensitivity reactions and neurotoxicity.^{3,8,9} Therefore, premedication with corticosteroids and antihistaminics are required. CrEL is also known to leach plasticizers from PVC administration sets, and for this reason PVC-free infusion bags are required.^{10,11} These drawbacks urge scientists to develop alternative formulations by which the use of CrEL would no longer be needed and the selectivity and potency toward cancer cells can be enhanced.¹²

Received: September 16, 2015

Revised: December 8, 2015

Published: December 9, 2015

Scheme 1. Schematic representation of Amphiphilic Block Copolymer Micelles That Self-Assemble in Aqueous Medium above the Phase Transition Temperature of One of the Polymer Blocks^a



^aThe hydrophobic cavity that is formed can be used for encapsulating hydrophobic drug molecules. Degradation of specific side chains in the temperature-responsive block leads to a polarity switch and renders the block copolymers fully water-soluble irrespective of temperature, thereby inducing drug release.

In the past decades nanoparticles, such as liposomes and polymer-based systems have been intensively investigated as drug delivery systems.^{13–16} Nanoparticles loaded with chemotherapeutic agents have several advantages compared with chemotherapeutics in soluble state. The major benefit is the ability to solubilize drug molecules and passively target them to tumors via the enhanced permeation and retention (EPR) effect.^{17–19} Tumors have a leaky tumor vasculature due to rapid angiogenesis, which supplies the tumor with oxygen and other nutrients and allows extravasation of nanoparticles in tumor tissue. Furthermore, poor lymphatic drainage allows the retention of accumulated nanoparticles in tumors, which leads to higher drug concentrations at the tumor site and hence increased therapeutic efficacy. Importantly, the encapsulation of hydrophobic drugs, like paclitaxel, in the core of the nanoparticles increases the solubility of the drug and consequently avoids the use of adjuvants like CrEL.

Accumulation at the tumor site is only possible if nanoparticles have long circulation behavior in the bloodstream.^{14,20} Conventional nanoparticles are subject to rapid clearance by the reticuloendothelial system (RES), which can be circumvented by grafting the surface of nanoparticles with nonionic, hydrophilic polymers. The most commonly applied polymer is poly(ethylene glycol) (PEG).²¹ PEG is an extensively used nontoxic polymer with unique physicochemical properties, such as high water solubility and large exclusion volume. PEG-coated nanoparticles impart stealth properties by inhibiting opsonization and subsequently enhancing circulation.^{22,23}

Among different polymer-based systems, amphiphilic block copolymers, composed of a hydrophilic and hydrophobic domains, show great potential because of their large solubilizing power and loading capacity.²⁴ In aqueous medium, the block copolymers self-assemble into micelles with a hydrophobic core, stabilized by a hydrophilic shell. The hydrophobic core is highly suitable for the incorporation of hydrophobic drugs, whereas the hydrophilic shell provides colloidal stability and the opportunity to attach targeting moieties, for example.²⁵ Many polymeric micelles are under clinical evaluation.²⁶

To enhance the bioavailability and release of drugs at the target site, stimuli-responsive properties can be incorporated into the polymers.^{27–30} The benefit of these so-called “smart materials” is their ability to respond to endogenous or exogenous stimuli (e.g., pH and temperature), which leads to a change in properties such as conformation, solubility, or hydrophobic/hydrophilic balance. Polymeric micelles based on temperature-responsive polymers have been extensively studied in recent years for their use as drug delivery systems. These polymers can exhibit a phase transition temperature (T_{CP}),

which means that below the T_{CP} the polymer is fully hydrated and thus soluble in water whereas above this temperature hydrogen bonds are disrupted, which results in collapse of the polymer. The most well-known thermoresponsive polymeric systems are based on poly(*N*-isopropylacrylamide) (pNIPAm) and Pluronics (e.g., PEG-*b*-PPO-*b*-PEG).^{31,32} PNIPAm has a T_{CP} around 32 °C, which is interesting for biomedical applications since the T_{CP} is a few degrees below body temperature. The T_{CP} of the polymer can be tailored by incorporating hydrophilic and hydrophobic monomers.^{33,34} A disadvantage however of PNIPAm for biomedical application is that it is not biodegradable and requires in addition thermal treatment (hypo- or hyperthermia) to induce drug release from PNIPAm based systems.³⁵ These issues can be alleviated by combining temperature-responsive behavior with a pH-triggered degradation mechanism that causes a switch in polarity.²⁸ Such systems are highly attractive for drug formulation and release under benign conditions (Scheme 1).

In this paper, we introduce a new class of degradable temperature-responsive polymers based on a simple modification of *N*-(2-hydroxypropyl)methacrylamide (HPMA). HPMA is hydrophilic and biocompatible, and polyHPMA has reached clinical trials as polymeric prodrug.^{36,16,37,38} We have modified HPMA with an ethyl group linked via a carbonate ester. Subsequently this monomer was polymerized by free radical polymerization (FRP) using a PEG-functionalized macroinitiator. The rationale of this strategy is that the introduced side chain will increase the hydrophobicity of the polymer and generate temperature-dependent solubility. Subsequent hydrolysis of the side chains will increase the hydrophilicity of the polymer and hence increase the T_{CP} . As a result, the polymer will gradually dissolve and thus provides an opportunity to be cleared from the body. We examined the self-assembly behavior and physicochemical properties of these polymers. *In vitro* cellular uptake was investigated in 2D and 3D cell cultures. Finally the potential of the polymer as anticancer drug carrier was evaluated, using paclitaxel as hydrophobic anticancer drug.

■ EXPERIMENTAL SECTION

Materials. *N*-(2-Hydroxypropyl)methacrylamide (HPMA) was obtained from Polysciences. Acetonitrile (ACN) was purchased from Acros Organics. A poly(ethylene glycol)-based macroinitiator, mPEG₂-ABCPA (M_n of mPEG = 5000 Da), was prepared as reported in literature.³⁵ All other chemicals were purchased from Sigma-Aldrich and used as received.

Paclitaxel (PTX) was obtained from LC Laboratories. Octadecyl rhodamine B chloride (R18), enzyme-free cell dissociation buffer, Dulbecco's modified Eagle medium (DMEM), fetal bovine serum (FBS), L-glutamine, sodium pyruvate, penicillin, streptomycin,

Hoechst and Alexa Fluor 647 phalloidin were obtained from Invitrogen. SKOV-3 cells and B16-cells were supplied by ATCC.

Instrumentation. ^1H -Nuclear magnetic resonance (NMR) spectra were recorded on a Bruker 300 MHz FT-NMR spectrometer using CDCl_3 and d_6 -DMSO as solvents. Chemical shifts (δ) are given in ppm relative to TMS.

Electron spray ionization-mass spectroscopy (ESI-MS) was carried out on a Waters LCT Premier XETM TOF mass spectrometer with a ZsprayTM source and ESI and modular LocksprayTM interface, coupled to a Waters alliance HPLC system.

Size exclusion chromatography (SEC) was performed on a Shimadzu 20A system, equipped with a 20A ISO-pump and a 20A refractive index detector (RID). Measurements were executed in *N,N*-dimethylacetamide (DMA) containing 50 mM LiBr at 50 °C with a flow rate of 0.700 mL/min. Calibration of the 2 PL 5 μm Mixed-D columns was done with polymethylmethacrylate (PMMA standards) obtained from PSS (Mainz).

Dynamic light scattering (DLS) was performed on a Zetasizer Nano S (Malvern) apparatus (Malvern Instruments Ltd.) at an angle of 173°.

For transmission electron microscopy (TEM), an aqueous micelle dispersion was deposited on a carbon coated copper grid and stained with uranyl acetate. TEM images were recorded with a JEOL 1010 TEM.

Fluorescence spectroscopy was carried out on a Cary Eclipse fluorescence spectrophotometer (Agilent Technologies) equipped with a Varian Cary temperature controller.

Confocal microscopy images were recorded on a Leica DMI6000 microscope coupled to an Andor DSD2 scanner and a Zyla5.5 CMOS camera. Two-dimensional cell cultures were imaged with a 1.40 NA, 63 \times oil immersion objective. Three-dimensional spheroids were imaged with a 10 \times objective. Images were processed with ImageJ.

Flow cytometry (FACS) was performed on a BD Accuri C6 (BD Biosciences). Data were processed with FLOWJO software.

Synthesis of HPMA-EC. The synthesis of HPMA-EC was performed in two steps and was based on the protocol for the synthesis of HEMA-Cl.³⁹ First, a round-bottom flask was filled with 1,1'-carbonyldiimidazole (CDI) (6.84 g, 45.0 mmol) and 40 mL of anhydrous dichloromethane under a nitrogen atmosphere. Subsequently, *N*-(2-hydroxypropyl)methacrylamide (HPMA) (4.296 g, 30.0 mmol) was added, after which a clear solution was obtained. After 2 h stirring at room temperature, the reaction mixture was transferred to a separatory funnel and washed with water. The dichloromethane layer was dried over MgSO_4 and filtered. The solvent was removed under reduced pressure, yielding the activated monomer as yellow oil (yield 89%). ^1H NMR (CDCl_3 , 300 MHz), δ (ppm): 8.09 (s, 1H, imi-H), 7.39 (s, 1H, imi-H), 7.05 (s, 1H, imi-H), 6.27 (br, 1H, $\text{CH}_2\text{NHC=O}$), 5.65 (m, 1H, C=CH_2), 5.33 (m, 1H, C=CH_2), 5.23–5.14 (m, 1H, CH=CH_3), 3.68–3.58 (m, 1H, NHCH_2), 3.56–3.47 (m, 1H, NHCH_2), 1.76 (s, 3H, $\text{CH}_3\text{C=CH}_2$), 1.44 (d, $J = 6.4$, 3H, CH=CH_3). ESI-MS $\text{C}_{11}\text{H}_{17}\text{N}_3\text{O}_3$: calculated $[\text{M} + \text{H}]^+$ 238.1192, $[\text{M} + \text{Na}]^+$ 260.1011, $[\text{M} + \text{K}]^+$ 276.0750; found $[\text{M} + \text{H}]^+$ 238.1183, $[\text{M} + \text{Na}]^+$ 260.1015, $[\text{M} + \text{K}]^+$ 276.0749.

In the next step, the activated monomer (2.0 g, 8.43 mmol) was dissolved in 10 mL of anhydrous ethanol (which is also the reactant for HPMA-EC) under a nitrogen atmosphere. *p*-Methoxyphenol (10 mg) was added to prevent autopolymerization. The reaction mixture was stirred overnight at 50 °C. Afterward the solvent was evaporated under reduced pressure, and the residual reaction mixture could be purified using silica gel column chromatography (eluent hexane/EtOAc, 3/7 (v/v)) (yield 67%). ^1H NMR (CDCl_3 , 300 MHz), δ (ppm) 6.23 (br, 1H, NHC=O), 5.67 (m, 1H, C=CH_2), 5.32 (m, 1H, C=CH_2), 4.88 (dq, 1H, $J = 7.4$, 6.4, 3.2 Hz, CH=CH_3), 4.18 (q, 2H, $J = 7.1$ Hz, $\text{CH}_2\text{=CH}_3$), 3.59 (ddd, 1H, $J = 14.4$, 6.0, 3.2 Hz, NHCH_2), 3.39 (ddd, 1H, $J = 14.4$, 7.4, 5.8 Hz, NHCH_2), 1.94 (m, 3H, $\text{CH}_3\text{C=CH}_2$), 1.29 (t, 3H, $J = 7.1$ Hz, $\text{CH}_2\text{=CH}_3$ and d, 3H, $J = 6.4$ Hz, CH=CH_3). ESI-MS $\text{C}_{16}\text{H}_{17}\text{NO}_4$: calculated $[\text{M} + \text{H}]^+$ 216.1236, $[\text{M} + \text{Na}]^+$ 238.1055, $[\text{M} + \text{K}]^+$ 254.0795; found $[\text{M} + \text{H}]^+$ 216.1235, $[\text{M} + \text{Na}]^+$ 238.1059, $[\text{M} + \text{K}]^+$ 254.0794.

Synthesis of PEG-Poly(HPMA-EC). Block copolymers of HPMA-EC and ethylene glycol were synthesized by free radical

polymerization. This was accomplished using a PEG-functionalized diazo(macro)initiator (mPEG5000-ABCPA)³⁵ with a molar ratio monomer/initiator of 150:1. First, monomer and macroinitiator were dissolved at a total concentration of 0.3 g/mL in anhydrous ACN. The mixture was degassed by three freeze–pump–thaw cycles, and the reaction was performed at 70 °C for 19 h under a nitrogen atmosphere. The obtained block copolymer was purified by precipitation in cold diethyl ether. After centrifugation, the residue was dried overnight under vacuum at room temperature. Finally, the polymer was dialyzed at 5 °C against water (MWCO 3.5 kDa) for 3 days and recollected after lyophilization. The block copolymer was analyzed by ^1H NMR and SEC. The dispersity of the block copolymer and PEG macroinitiator and block copolymer individually is calculated as 5.4 and 1.9, respectively. A conversion of 95% was observed, determined by ^1H NMR as follows:

$$\text{Conversion (\%)} = 100 \times (1 - [(A_{\text{monomer}}/n)/(A_{\text{polymer}}/n)])$$

Determination of Cloud Point (CP). The cloud point (CP) of the block copolymer in aqueous solution was investigated by DLS. First the block copolymer was dissolved in ice-cold deionized water at a concentration of 5 mg/mL. The sample was then heated from 5 to 40 °C using a 1 °C interval. During heating, the size and scattering intensity were measured in quadruple. The CP was estimated as the onset on the X-axis obtained by extrapolation of the scattering intensity–temperature curve to intensity baseline.

Particle Size and Hydrolysis. Particle size was measured by DLS in deionized water at a concentration of 5 mg/mL. For monitoring particle size during hydrolysis of the carbonate ester moieties, the block copolymer was dissolved at 5 mg/mL in an aqueous 0.1 M NaOH solution. Subsequently, the size and scattering intensity were measured at 37 °C in 15 min intervals.

Critical Micelle Concentration (CMC). Pyrene (12 $\times 10^{-5}$ mg/mL) and block copolymers (concentration range from 0.001 to 1 mg/mL) were dissolved in deionized water and measured at room temperature. Fluorescence excitation spectra were recorded with an excitation wavelength of 390 nm and monitored from 300 to 360 nm. The CMC was determined based on the change in excitation intensity of ratio at 338 and 333 nm of pyrene in function of the block concentrations.⁴⁰

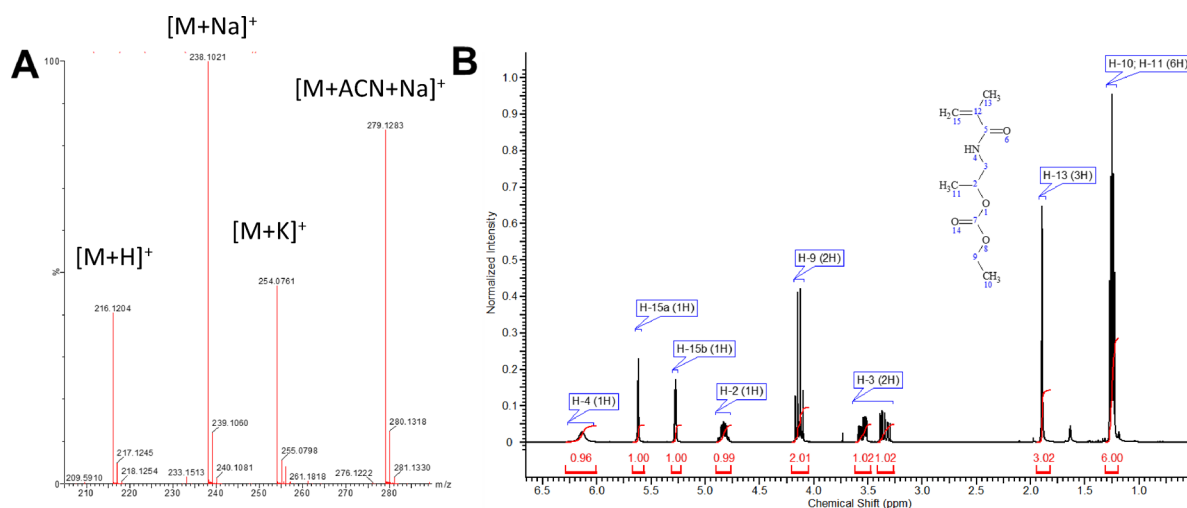
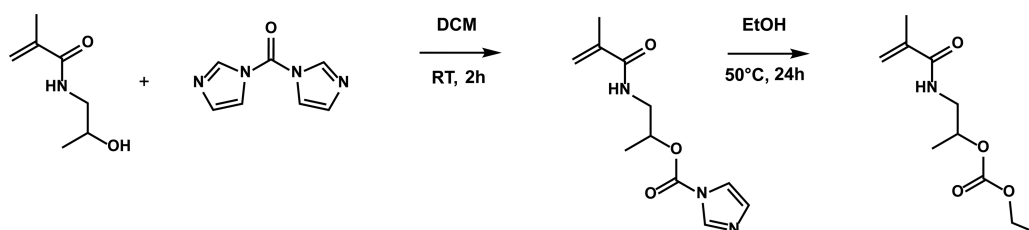
In Vitro Cell Culture Experiments. SKOV-3 (human ovarian cancer cell line) cells and B16.F10 (mouse melanoma cells) were cultured in DMEM supplemented with 10% FBS, 2 mM L-glutamine, 1 mM sodium pyruvate, and antibiotics (50 units/mL penicillin and 50 $\mu\text{g/mL}$ streptomycin). Cells were incubated at 37 °C in a controlled, sterile environment of 95% relative humidity and 5% CO_2 . Micelles were loaded with the hydrophobic fluorescent dye rhodamine B octadecyl ester by adding a small amount (20 μL) of a concentrated ethanolic solution (1 mg/mL) to the block copolymer dispersion in cold water (10 mg/mL) under stirring. As a control, the same ethanolic solution was added to pure water, leading to precipitation of the hydrophobic dye. Formulations were stabilized overnight at room temperature to allow evaporation of ethanol. The excess dye was removed by membrane filtration (0.450 μm).

For flow cytometry, cells were plated at a density of 10^5 cells per well in a 24 well plate and allowed to adhere overnight. Subsequently, cells were pulsed overnight with different concentrations (0.1, 0.2, and 0.5 mg/mL) of micelles. Next, wells were washed with PBS, detached from the plates with trypsin-free cell dissociation buffer and analyzed by flow cytometry.

For microscopy, cells were plated in WillCo Wells dishes at a density of 50×10^4 cells per well and allowed to adhere overnight. Subsequently, cells were pulsed overnight with micelles, 10 μL of 10 mg/mL R18-labeled PEG-poly(HPMA-EC), followed by washing with PBS and fixation with 4% paraformaldehyde. Prior to imaging, cell nuclei were stained with Hoechst 33342 (according to manufacturers protocol), and the cell membrane was stained with AlexaFluor488-conjugated phalloidin.

Three-Dimensional Spheroids. The human breast cancer cell line MCF-7 (ATCC, Manassas, VA) was stably transfected with an

Scheme 2. Synthesis of Ethyl(1-methacrylamidopropan-2-yl)carbonate (HPMA-EC)

Figure 1. (A) MS and (B) ^1H NMR spectra confirm successful synthesis of HPMA-EC.

empty peGFP-c1 vector (Clontech, Mountain View, CA) (MCF-7 GFP) as described previously.⁴¹ The cell line was maintained in DMEM supplemented with 10% FBS, 100 U/mL penicillin, 100 mg/mL streptomycin, and 1 mg/mL G418 and incubated at 37 °C, 10% CO_2 . Cells were grown in adherent conditions to 70% confluency, trypsinized, counted (Countess automatic cell counter, Invitrogen), and adjusted to 10^5 cells/mL. Cell suspensions of 5 mL were incubated at 37 °C, 10% CO_2 under continuous gyratory shaking (50 rpm) to allow spheroid formation. After 72 h, 1 mL of R18 loaded PEG–poly(HPMA-EC) micelles was added to the spheroid suspensions, followed by incubation for 1, 4, or 7 days. At these time points, spheroids were collected and fixed in paraformaldehyde for examination by confocal microscopy. Image analysis was performed with the open source ImageJ software package.

Drug Loading. Paclitaxel (PTX) loading was performed according to Shi et al.⁴² A 1 mg/mL solution of PTX in ethanol was prepared, and 100 μL of this solution was added to 1 mL of a 5 mg/mL PEG–poly(HPMA-EC) solution in cold (5 °C) water followed by rapid heating to 50 °C to allow for micelle formation. The formulation was allowed to stabilize overnight at room temperature, with the lid kept open to enable evaporation of the ethanol.

In Vitro Cytotoxicity Assay. *In vitro* cytotoxicity was determined using the 3-(4,5-dimethylthiazol-2-yl)-2,5-diphenyltetrazolium bromide (MTT) assay as described earlier by Louage et al.⁴³ SKOV-3 cells were pulsed with different concentrations of PTX loaded PEG–poly(HPMA-EC) micelles and a control nanoparticle formulation, Genexol-PM (Samyang Biopharmaceuticals). The MTT stock solution was prepared by dissolving 100 mg of MTT in 20 mL of PBS and subsequent membrane filtration (0.22 μm). Before use, the MTT stock solution was 5-fold diluted with culture medium.

SKOV-3 cells were seeded into 96-well titer plates (10000 cells per well, suspended in 200 μL of culture medium) and incubated overnight. Next, 50 μL of sample, DMSO (positive control = 0% viability) or water (negative control = 100% viability) was added to the cells, followed by 72 h of incubation. Subsequently, the medium was aspirated, and the cells were washed with 250 μL of PBS. After

aspiration, 100 μL of MTT working solution was added, and the cells were incubated for 2.5 h. Finally, the MTT working solution was aspirated and the formed purple formazan crystals were dissolved in 50 μL of DMSO. Absorbance was determined at 590 nm using an EnVision Multilabel plate reader. The absorbance of the positive control was used as a blank and therefore subtracted from all values. The dilution series and positive and negative control were added to the wells in triplicate ($n = 3$). Cell viability (%) was calculated according to the equation below.

$$\text{Cell viability} = \frac{\text{Abs}(\text{sample}) - \text{Abs}(+\text{control})}{\text{Abs}(-\text{control}) - \text{Abs}(+\text{control})} \times 100\%$$

RESULTS AND DISCUSSION

HPMA was modified with an ethyl group via a carbonate ester (Scheme 2). In the first step, the secondary hydroxyl group of HPMA was activated by 1,1'-carbonyldiimidazole (CDI), thereby yielding 1-methacrylamidopropan-2-yl 1H-imidazole-1-carboxylate (HPMA-CI) (Figures 1SI and 2SI, Supporting Information). In a second step, the imidazole group was substituted by ethanol, yielding ethyl (1-methacrylamidopropan-2-yl) carbonate, which is further denoted as HPMA-EC. The attractiveness of this route lies in the fact that no additional catalyst is required and final workup is very straightforward. Indeed, in the second step of the reaction, ethanol, which is the reactant itself, was used as solvent, and the excess could easily be removed by rotary evaporation. Moreover, no additional catalyst was required because the reaction is base catalyzed by the imidazole that is formed as byproduct. Finally, HPMA-ethylcarbonate (HPMA-EC) could easily be purified and isolated by flash chromatography that only needs to remove imidazole and a small fraction of hydrolyzed HPMA, which both have a very distinct polarity compared with HPMA-EC.

Scheme 3. Synthesis Route of PEG–PolyHPMA-EC by Free Radical Polymerization

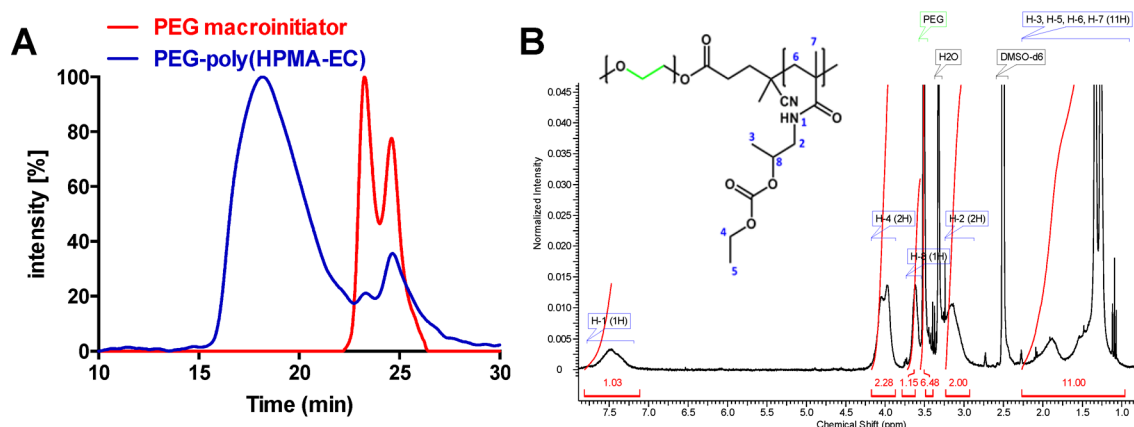
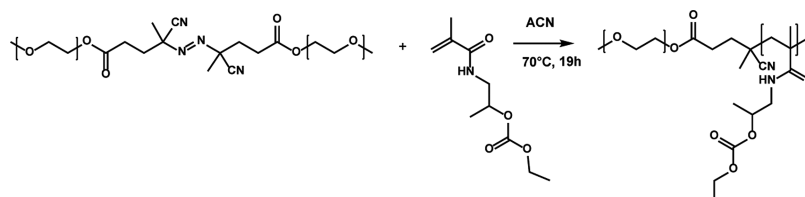


Figure 2. (A) PEG-MI gives rise to two peaks, which correspond to mono- and bifunctional initiator (red curve). After polymerization, a new peak with a shorter retention time emerges, which provides evidence of successful block copolymerization (blue curve). (B) ^1H NMR spectrum after block copolymerization.

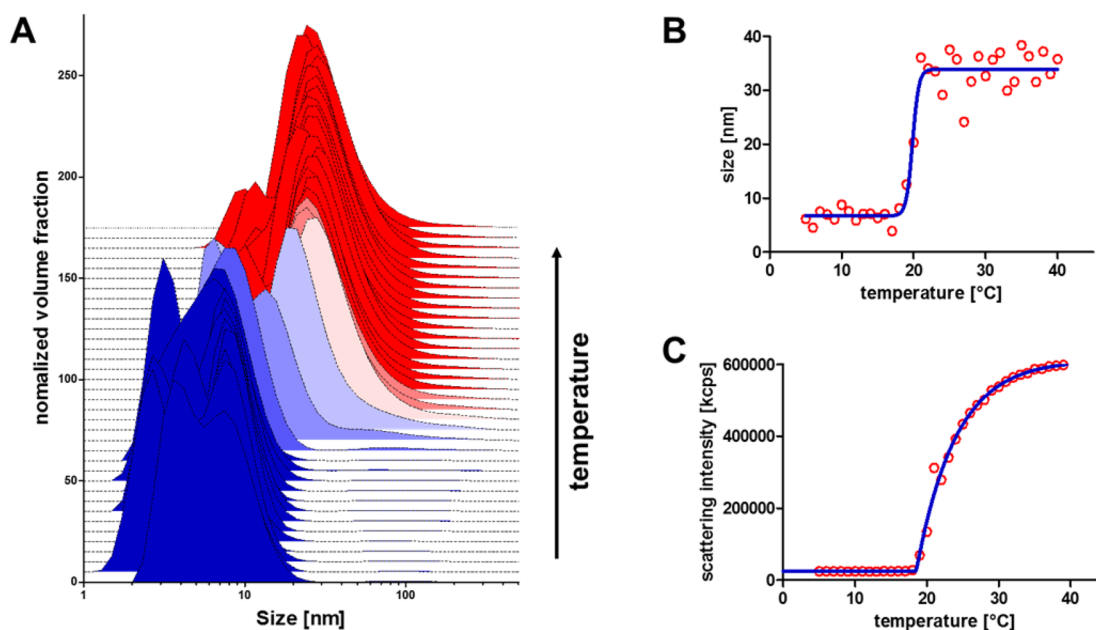


Figure 3. Evolution of particle size distribution (A), mean diameter (B), and light scattering intensity (C) as a function of temperature, measured by DLS.

The ^1H NMR and ESI-MS spectra of the HPMA-EC are shown in Figure 1 and confirm successful synthesis of the monomer. The straightforward synthesis and purification procedure to produce the HPMA-EC monomer could be considered as advantageous over other more elaborate procedures to modify HPMA with hydrolyzable hydrophobic moieties such as lactates. Indeed, to produce the latter, preparative HPLC is required to separate HPMA modified with oligomers of different length. Furthermore, hydrolysis of the carbonate esters liberates CO_2 and ethanol as byproducts and does not

induce local acidification as is the case for lactate based materials that liberate lactic acid upon hydrolysis. Besides methacrylamides, we also attempted the CDI route for acrylates (i.e., 2-hydroxyethyl acrylate, HEA) and acrylamides (i.e., 2-hydroxyethylacrylamide, HEAM). However, according to MS, this was unsuccessful most likely due to Michael addition between the acrylate and acrylamide moieties and the secondary amines of the imidazole byproduct during both reaction steps (Figure 3SI, Supporting Information); that is why HPMA was opted for further investigation.

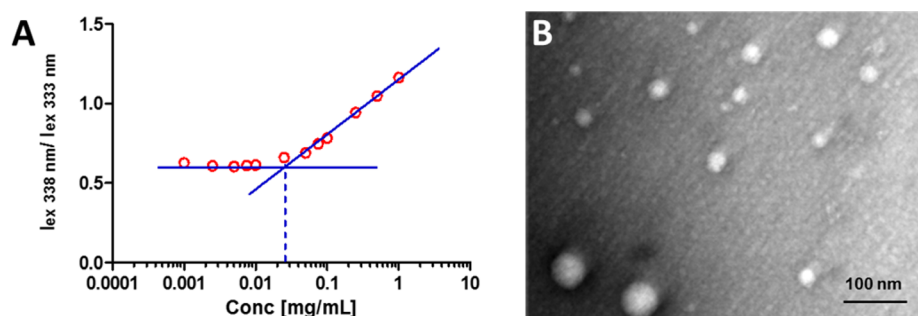


Figure 4. (A) Critical micelle concentration in PBS, determined by measuring the excitation intensity ratio of pyrene at 338 nm (I_3) and 333 nm (I_1) as a function of PEG–poly(HPMA-EC) concentration by fluorescence spectroscopy at 37 °C. (B) Transmission electron microscopy (TEM) image of PEG–poly(HPMA-EC) micelles. A negative staining was used to visualize the micelles.

Next, we aimed at using the HPMA-EC for the synthesis of amphiphilic block copolymers. For this purpose, we used a 5 kDa PEG-macroinitiator³⁵ and polymerized HPMA-EC via free radical polymerization (FRP) in acetonitrile (ACN). Scheme 3 depicts the synthesis route of PEG–polyHPMA-EC, and Figure 2A shows the SEC traces before and after the polymerization reaction. The PEG macroinitiator gives rise to two peaks, which correspond to mono- and bisfunctional initiator. After polymerization, a new peak with a shorter retention time emerges, indicating the formation of PEG–poly(HPMA-EC) block copolymer. ¹H NMR (Figure 2B) provided further proof of successful polymerization. After polymerization, the characteristic vinyl protons nearly fully disappeared. The small amount of residual monomer was removed by dialysis against water. The number-average molar weight (M_n) of the block copolymer calculated by ¹H NMR is approximately 20 kDa. GPC analysis calculated a M_n of 136 kDa and a \bar{D} (M_w/M_n) of 1.9. (Figure 4SI, Supporting Information). The discrepancy between NMR and GPC results can likely be attributed to the presence of a fraction of unreacted PEG-macroinitiator that leads to an underestimation of the molecular weight by NMR. Besides that, the hydrodynamic behavior of the PEG–poly(HPMA-EC) block copolymer is likely very different from the PMMA standards that were used to calibrate the GPC.

The micellization and temperature-responsive behavior of the PEG–poly(HPMA-EC) block copolymer was investigated by dynamic light scattering (DLS). We observed that at room temperature the block copolymer spontaneously formed micelles in aqueous medium and required cooling to fully solubilize. Figure 3 depicts the evolution of particle size and light scattering intensity as a function of temperature. These data show that below 17 °C the block copolymers exist as soluble unimers, whereas from 17 °C onward, micelles are formed with diameter of around 40 nm. Figure 5SI (Supporting Information) depicts the size distribution of the micelles at 37 °C, clearly depicting the formation of monomodal nanoparticles. These data confirm our hypothesis that pHPMA-EC exerts temperature-responsive behavior. Moreover, the phase transition temperature of 17 °C is within an attractive range for drug delivery purposes, because it is below room temperature, which allows easy handling of the block copolymers in stable micellar state at room temperature, whereas the polymer can readily be dissolved at a mildly lower temperature. Next we determined the critical micelle concentration of the PEG–poly(HPMA-EC) in aqueous medium at 37 °C using the pyrene assay. Figure 4A plots the excitation ratio of pyrene at 338 nm (I_3) and 333 nm (I_1) versus polymer concentration.

Plotting the crossing of both tangent curves yields a CMC of 0.025 mg/mL, which is comparable to mPEG-*b*-(HPMAm-Lac)₂⁴⁴ and PEG–PLA block copolymers.⁴⁵ Further proof of micelle formation was gained by transmission electron microscopy (TEM; Figure 4B), which clearly shows the presence of particulate structures.

The ability of the PEG–poly(HPMA-EC) micelles to disassemble in aqueous medium by hydrolytic degradation of the carbonate ester, which connects the HPMA backbone to the pending ethyl side chains, was examined. As a proof of concept, we performed these experiments in aqueous 0.1 M NaOH solution to accelerate the degradation rate of the carbonate esters, which allows real-time monitoring by DLS of the evolution in particle size and scattering intensity over time (Figure 5). In a first phase, particle size increases due to particle

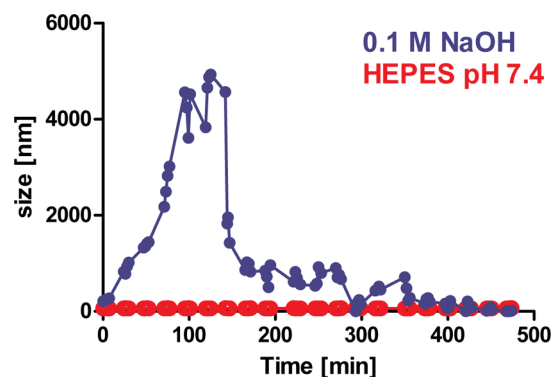


Figure 5. Evolution of particle size as a function of degradation time in response to basic pH (i.e., 0.1 M NaOH) and physiological pH (Hepes buffer, pH 7.4).

swelling or the formation of loose aggregates. In a second phase, particle size rapidly drops until soluble unimers are measured. These data are in agreement with those of Soga et al. on pHPMA-Lac micelles⁴⁴ and show that the PEG–poly(HPMA-EC) micelles can be disintegrated in response to basic pH. At physiological pH of 7.4 in HEPES buffer, the micelles remain invariant over the studied time course. Slow degradation at neutral pH values have been reported by others,¹⁶ and future research efforts will explore the possibility to accelerate the hydrolysis of the carbonate ester bond using primary alcohols instead of secondary for carbonate modification.

To investigate the ability of the block copolymer micelles to deliver a hydrophobic drug payload into living cells, we loaded them with the red fluorescent hydrophobic dye rhodamine octadecylester (R18). When R18 is added from a concentrated

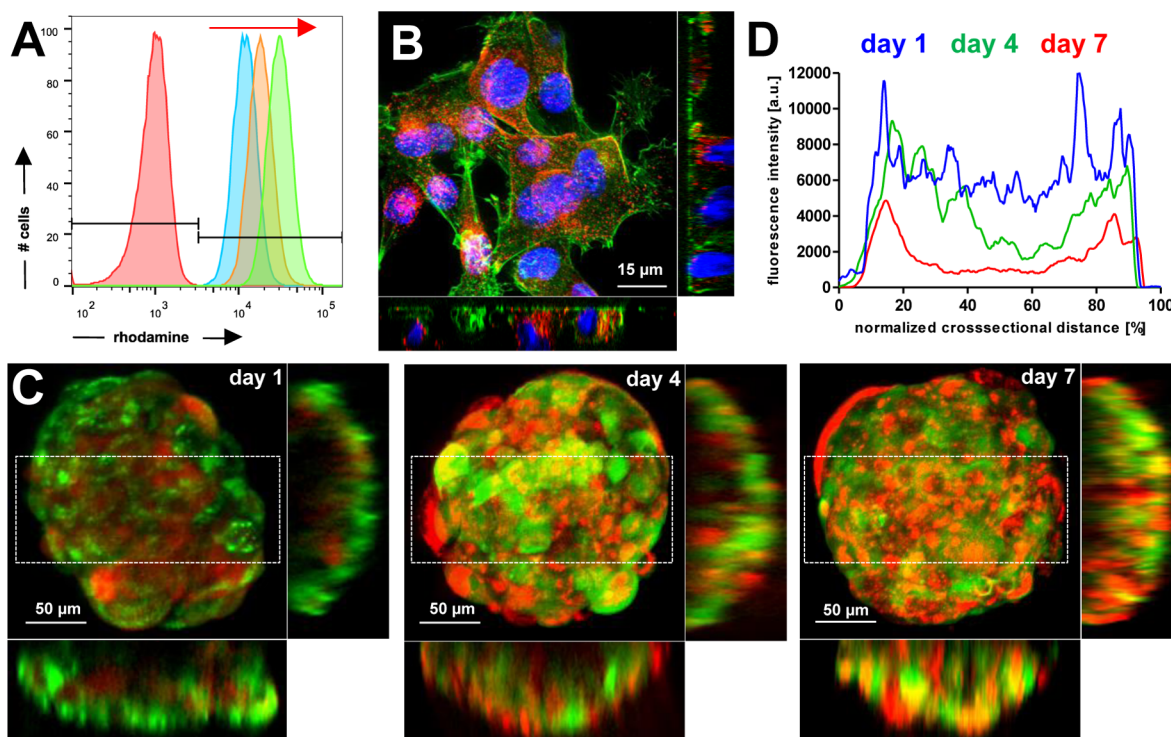


Figure 6. (A) Flow cytometry histograms of B16.F10 cells incubated with different doses (0.1, 0.2 and 0.5 mg/mL) of R18 loaded PEG-poly(HPMA-EC) micelles. (B) Confocal microscopy image (maximum intensity projection (MIP) and orthogonal planes) of B16.F10 melanoma cells pulsed with rhodamine loaded PEG-poly(HPMA-EC) micelles (red fluorescence). Cell nuclei were stained blue with Hoechst, and cell membrane was stained green with AlexaFluor488 conjugated phalloidin. (C) Confocal microscopy image (maximum intensity projection (MIP) and orthogonal planes) of eGFP-expressing MCF-7 human breast cancer cells (green fluorescence) incubated with rhodamine loaded PEG-poly(HPMA-EC) micelles (red fluorescence). The image shows penetration into the different layers of the sphere, and intracellular uptake is characterized by the yellow color, due to colocalization of GFP with the rhodamine (especially notable at day 7). (D) Semiquantitative analysis of rhodamine by software integration of the rectangular areas marked in the panels C.

(10 mg/mL) solution into pure water (i.e., a process called solvent displacement), immediate precipitation of the dye occurred. However, when R18 was added to an aqueous solution of PEG-poly(HPMA-EC), a stable pinkish translucent solution was obtained. Subsequently, we incubated B16.F10 mouse melanoma cells with different doses of R18 loaded micelles followed by flow cytometry (FACS) analysis. As shown in Figure 6A, a dose-dependent cellular association is observed, whereas R18 in the control samples (did not show any cellular association). To elucidate whether the block copolymer micelles are internalized by cells or only adhering to the cell membrane, confocal microscopy was performed. Cell nuclei were counterstained with Hoechst (blue fluorescence), and the cell membrane was stained with AlexaFluor488-conjugated phalloidin. The maximum intensity projection (Figure 6B) and the corresponding orthogonal projections clearly show that the micelles can efficiently deliver a hydrophobic payload inside cells.

It has been reported by the Kataoka group that efficient delivery of drug loaded nanoparticles into solid tumors is strongly dependent on particle size with sub-50 nm particles offering optimal tumor penetration.⁴⁶ In this regard, we aimed at screening the ability of our block copolymer nanoparticles to deliver a hydrophobic payload into cancer cell spheroids. These are 3D spherical structures that are an *in vitro* mimicry of a solid tumor.⁴⁷ Spheroids were grown from eGFP-expressing MCF-7 human breast cancer cells and incubated for 7 days with R18-loaded micelles. After 1, 4, and 7 days, spheroids were harvested and fixed with paraformaldehyde (PFA). Subsequently, the

spheroids were imaged in 3D by confocal microscopy. As depicted in Figure 6C, after 1 day of incubation, the red fluorescence from the micelles was distributed mainly in the periphery of the spheroids. After 4 days, the hydrophobic payload has penetrated more deeply into the spheroids, whereas after 7 days the punctuated fluorescence pattern was visible throughout the whole volume of the spheroids. Semiquantitative analysis of the rhodamine penetration depth in the spheroids for the different time points confirms the gradual infiltration of the spheroids from the periphery at day 1 until a more or less homogeneous distribution throughout the interior of the spheroids is obtained at day 7. These data suggest that the micelles are capable of diffusing into 3D cancer cell cultures and hold promise for drug delivery to tumors *in vivo*, too.

To investigate whether PEG-poly(HPMA-EC) micelles are capable of enhancing the cellular uptake of a hydrophobic anticancer drug, we loaded them with paclitaxel (PTX) by adding 100 μ L of an ethanol PTX (1 mg/mL) solution to an aqueous solution of PEG-poly(HPMA-EC) (5 mg/mL) below the T_{cp} of the polymer followed by rapid heating of the solution to 50 $^{\circ}$ C. The latter procedure has been reported by the Hennink group as a straightforward route to obtain optimal encapsulation of hydrophobic drugs into temperature responsive block copolymer micelles.⁴⁸ The conditions for drug loading were based on initial screening experiments in which we added different amounts of PTX to a PEG-poly(HPMA-EC) micelle solution followed by analysis by polarized light microscopy and DLS to detect from which concentration

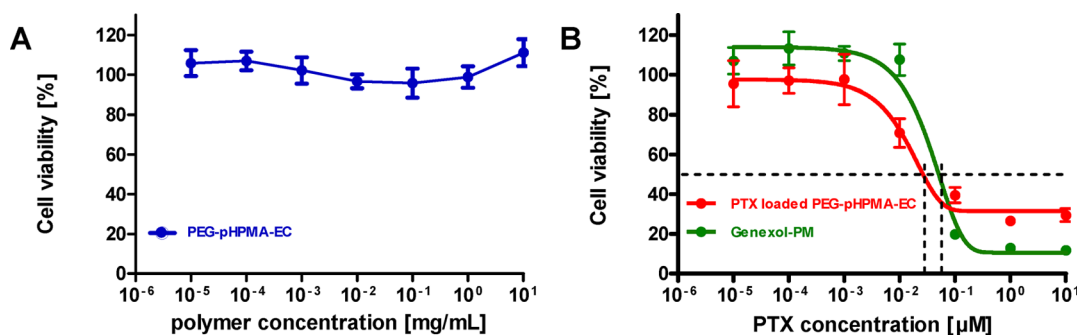


Figure 7. Cell viability measured by MTT assay of SKOV-3 cells that were treated with different doses of (A) unloaded PEG–poly(HPMA-EC) and (B) paclitaxel (PTX) loaded PEG–poly(HPMA-EC) micelles after 72 h of incubation. Genexol-PM was used as control nanoformulation ($n = 3$).

onward precipitation of nonstabilized PTX occurs. Subsequently, the PTX concentration for further *in vitro* experiments was chosen well below the regime in which PTX precipitates. SKOV-3 cells were pulsed with a concentration series of PTX–PEG–poly(HPMA-EC) and with Genexol-PM as control nanoformulation. Genexol-PM is PTX-loaded PEG–poly(lactide) block copolymer micelles.⁴⁹ The inhibitory effect on cancer cell growth of these formulations over 72 h was determined using the MTT assay. Cells were also incubated with empty PEG–poly(HPMA-EC) micelles to assess possible toxicity of the polymer itself. As shown in Figure 7, no intrinsic toxicity of the polymer could be observed within the tested concentration range, indicating that the synthesized polymeric micelle carrier is cytocompatible at least within this experimental window. PTX-loaded PEG–poly(HPMA-EC) micelles, by contrast, show dose-dependent cytotoxicity similar to Genexol-PM. Both PEG–poly(HPMA-EC) and Genexol-PM micelles will not be fully hydrolyzed over the time course of this *in vitro* experiment. This suggests that drug release is, at least in part, independent of the degradation of the hydrophobic micelle core but rather occurs through a combination of the dilution effect and affinity of the drug for other hydrophobic binding sites in the cell culture medium or within the cell.

CONCLUSIONS

In conclusion, we have proposed in this paper a straightforward route for hydrophobic modification of the monomer HPMA that is frequently investigated for biomedical applications. Grafting an ethyl moiety to the pending OH group of HPMA via a hydrolytically sensitive carbonate ester, we showed that this monomer could be used for the synthesis of degradable temperature-responsive block copolymers using a PEG-macro-initiator strategy. These block copolymers formed micellar nanoparticles in aqueous medium that efficiently encapsulated hydrophobic compounds and delivered these to 2D and 3D cancer cell cultures. Finally we showed that these block copolymers could formulate the anticancer drug paclitaxel and induce cytotoxicity *in vitro*. Our ongoing research focuses on exploring other side groups than ethyl for HPMA modification and accelerating the degradation rate of the carbonate esters by introduction of the carbonate ester onto a primary instead of a secondary alcohol. Furthermore, micelle cross-linking, stabilization by secondary interactions, and covalent drug loading will be investigated to increase the stability of the nanoformulation in the bloodstream at high dilution and in the presence of proteins. Finally, we are also focusing on controlled radical polymerizations such as RAFT, which are favored to obtain

control over the polymeric chain ends for additional introduction of targeting moieties. Taken together, the main novelty of our present work is the straightforward synthesis and purification of an HPMA derivative that yields degradable temperature-responsive polymers with benign degradation byproducts. Such systems are attractive for drug delivery purposes. Indeed, simple heating above their phase transition temperature leads to self-assembly and the formation of hydrophobic domains that can be exploited to solubilize hydrophobic drug molecules, as illustrated in this paper for paclitaxel.

ASSOCIATED CONTENT

Supporting Information

The Supporting Information is available free of charge on the ACS Publications website at DOI: 10.1021/acs.biomac.5b01252.

Additional experimental data (PDF)

AUTHOR INFORMATION

Corresponding Author

*Prof. Dr. Bruno G. De Geest. Mailing address: Department of Pharmaceutics, Ghent University Ottergemsesteenweg 460, 9000 Ghent, Belgium. E-mail: br.degeest@ugent.be. Phone: +32 9 264 80 55.

Author Contributions

The manuscript was written through contributions of all authors. All authors have given approval to the final version of the manuscript. S.K. and B.L. contributed equally.

Notes

The authors declare no competing financial interest.

ACKNOWLEDGMENTS

B.L. acknowledges the IWT-Flanders for a Ph.D. scholarship. B.D.G. and R.H. acknowledge the FWO-Flanders for funding.

REFERENCES

- (1) Steichen, S. D.; Caldorera-Moore, M.; Peppas, N. a. *Eur. J. Pharm. Sci.* **2013**, *48* (3), 416–427.
- (2) Oerlemans, C.; Bult, W.; Bos, M.; Storm, G.; Nijssen, J. F. W.; Hennink, W. E. *Pharm. Res.* **2010**, *27* (12), 2569–2589.
- (3) Gelderblom, H.; Verweij, J.; Nooter, K.; Sparreboom, a. *Eur. J. Cancer* **2001**, *37* (13), 1590–1598.
- (4) Chen, H.; Khemtong, C.; Yang, X.; Chang, X.; Gao, J. *Drug Discovery Today* **2011**, *16* (7–8), 354–360.
- (5) Singla, A. K.; Garg, A.; Aggarwal, D. *Int. J. Pharm.* **2002**, *235* (1–2), 179–192.
- (6) Panchagnula, R. *Int. J. Pharm.* **1998**, *172* (1–2), 1–15.

- (7) Mu, L.; Feng, S. S. *J. Controlled Release* **2003**, *86* (1), 33–48.
- (8) Szebeni, J.; Muggia, F. M.; Alving, C. R. *J. Natl. Cancer Inst.* **1998**, *90* (4), 300–306.
- (9) Kimura, K.; Ohno, R.; Amaki, I.; Hattori, K.; Hirota, Y.; Hoshino, A.; Ichimaru, M.; Ito, M.; Kimura, I.; Maekawa, T. *Med. Oncol. Tumor Pharmacother.* **1987**, *47* (9), 2486–2493.
- (10) Pawar, R.; Shikanov, A.; Vaisman, B.; Domb, A. J. *Curr. Med. Chem.* **2004**, *11* (4), 397–402.
- (11) Moreno-Aspitia, A.; Perez, E. A. *Future Oncol.* **2005**, *1* (6), 755–762.
- (12) Ta-Chung, C.; Chu, Z.; Tseng, L. M.; Chiou, T. J.; Hsieh, R. K.; Wang, W. S.; Yen, C. C.; Yang, M. H.; Hsiao, L. T.; Liu, J. H.; Chen, P. M. *Invest. New Drugs* **2005**, *23* (2), 171–177.
- (13) Ahmad, Z.; Shah, A.; Siddiq, M.; Kraatz, H.-B. *RSC Adv.* **2014**, *4* (33), 17028–17038.
- (14) Brannon-Peppas, L.; Blanchette, J. O. *Adv. Drug Delivery Rev.* **2004**, *56* (11), 1649–1659.
- (15) Pillai, G. J. *Pharm. Pharm. Sci.* **2014**, *1* (2), 1–13.
- (16) Soga, O.; van Nostrum, C. F.; Hennink, W. E. *Biomacromolecules* **2004**, *5* (3), 818–821.
- (17) Maeda, H.; Nakamura, H.; Fang, J. *Adv. Drug Delivery Rev.* **2013**, *65* (1), 71–79.
- (18) Fang, J.; Nakamura, H.; Maeda, H. *Adv. Drug Delivery Rev.* **2011**, *63* (3), 136–151.
- (19) Maeda, H.; Wu, J.; Sawa, T.; Matsumura, Y.; Hori, K. *J. Controlled Release* **2000**, *65* (1–2), 271–284.
- (20) Brigger, I.; Dubernet, C.; Couvreur, P. *Adv. Drug Delivery Rev.* **2002**, *54* (5), 631–651.
- (21) Knop, K.; Hoogenboom, R.; Fischer, D.; Schubert, U. S. *Angew. Chem., Int. Ed.* **2010**, *49* (36), 6288–6308.
- (22) Li, S. D.; Huang, L. J. *Controlled Release* **2010**, *145* (3), 178–181.
- (23) Owens, D. E., III; Peppas, N. a. *Int. J. Pharm.* **2006**, *307* (1), 93–102.
- (24) Soga, O.; Van Nostrum, C. F.; Fens, M.; Rijcken, C. J. F.; Schiffellers, R. M.; Storm, G.; Hennink, W. E. *J. Controlled Release* **2005**, *103* (2), 341–353.
- (25) Deng, C.; Jiang, Y.; Cheng, R.; Meng, F.; Zhong, Z. *Nano Today* **2012**, *7* (5), 467–480.
- (26) Cabral, H.; Kataoka, K. *J. Controlled Release* **2014**, *190*, 465–476.
- (27) Ganta, S.; Devalapally, H.; Shahiwala, A.; Amiji, M. J. *Controlled Release* **2008**, *126* (3), 187–204.
- (28) Schmaljohann, D. *Adv. Drug Delivery Rev.* **2006**, *58* (15), 1655–1670.
- (29) Talelli, M.; Hennink, W. E. *Nanomedicine* **2011**, *6* (7), 1245–1255.
- (30) Rijcken, C. J. F.; Soga, O.; Hennink, W. E.; Nostrum, C. F. V. *J. Controlled Release* **2007**, *120* (3), 131–148.
- (31) Roy, D.; Brooks, W. L.; Sumerlin, B. S. *Chem. Soc. Rev.* **2013**, *42* (17), 7214–7243.
- (32) Ward, M. a.; Georgiou, T. K. *Polymers (Basel, Switz.)* **2011**, *3* (3), 1215–1242.
- (33) Feil, H.; Bae, Y. H.; Feijen, J.; Kim, S. W. *Macromolecules* **1993**, *26* (10), 2496–2500.
- (34) Shibayama, M.; Mizutani, S.; Nomura, S. *Macromolecules* **1996**, *29* (6), 2019–2024.
- (35) Neradovic, D.; van Nostrum, C. F.; Hennink, W. E. *Macromolecules* **2001**, *34* (22), 7589–7591.
- (36) Ulbrich, K.; Šubr, V. *Adv. Drug Delivery Rev.* **2010**, *62* (2), 150–166.
- (37) Talelli, M.; Rijcken, C. J. F.; van Nostrum, C. F.; Storm, G.; Hennink, W. E. *Adv. Drug Delivery Rev.* **2010**, *62* (2), 231–239.
- (38) Kopeček, J.; Kopečková, P. *Adv. Drug Delivery Rev.* **2010**, *62* (2), 122–149.
- (39) vanDijkWolthuis, W. N. E.; vanSteenbergen, M. J.; Underberg, W. J. M.; Hennink, W. E. *J. Pharm. Sci.* **1997**, *86* (4), 413–417.
- (40) Zhao, C.; Winnik, M. A.; Croucher, M. D.; Riess, G. *Langmuir* **1990**, *6* (2), 514–516.
- (41) Hendrix, A.; Maynard, D.; Pauwels, P.; Braems, G.; Denys, H.; Van Den Broecke, R.; Lambert, J.; Van Belle, S.; Cocquyt, V.; Gespach, C.; Bracke, M.; Seabra, M. C.; Gahl, W. a.; De Wever, O.; Westbroek, W. *J. Natl. Cancer Inst.* **2010**, *102* (12), 866–880.
- (42) Shi, Y.; Van Den Dungen, E. T. a.; Klumperman, B.; Van Nostrum, C. F.; Hennink, W. E. *ACS Macro Lett.* **2013**, *2* (5), 403–408.
- (43) Louage, B.; Zhang, Q.; Vanparijs, N.; Voorhaar, L.; Shi, Y.; Hennink, W. E.; Van Bocxlaer, J.; Hoogenboom, R.; De Geest, B. G.; Vande Castele, S. *Biomacromolecules* **2015**, *16* (1), 336–350.
- (44) Soga, O.; van Nostrum, C. F.; Ramzi, A.; Visser, T.; Soulimani, F.; Frederik, P. M.; Bomans, P. H. H.; Hennink, W. E. *Langmuir* **2004**, *20* (21), 9388–9395.
- (45) Zhao, H.; Liu, Z.; Piao, L.; et al. *Bull. Korean Chem. Soc.* **2012**, *33* (5), 1638–1642.
- (46) Cabral, H.; Matsumoto, Y.; Mizuno, K.; Chen, Q.; Murakami, M.; Kimura, M.; Terada, Y.; Kano, M. R.; Miyazono, K.; Uesaka, M.; Nishiyama, N.; Kataoka, K. *Nat. Nanotechnol.* **2011**, *6* (12), 815–823.
- (47) Sutherland, R. M. *Science* **1988**, *240* (4849), 177–184.
- (48) Neradovic, D.; Soga, O.; Van Nostrum, C. F.; Hennink, W. E. *Biomaterials* **2004**, *25* (12), 2409–2418.
- (49) Werner, M. E.; Cummings, N. D.; Sethi, M.; Wang, E. C.; Sukumar, R.; Moore, D. T.; Wang, A. Z. *Int. J. Radiat. Oncol., Biol., Phys.* **2013**, *86* (3), 463–468.